Available online at www.sciencedirect.com

ScienceDirect

Procedia IUTAM 22 (2017) 168 – 175

Procedia IUTAM

www.elsevier.com/locate/procedia

IUTAM Symposium on Nonlinear and Delayed Dynamics of Mechatronic Systems

Galerkin approximations for thermoacoustic instability in a Rijke's tube

Shanti Swaroop Kandala[a], Abhivamshi Maduri[a], C. P. Vyasarayani[a,*]

[a]*Department of Mechanical and Aerospace Engineering, Indian Institute of Technology Hyderabad, Kandi, Sanga Reddy - 502285, Telangana, India*

Abstract

A simple mathematical model for thermoacoustic instability (TAI) in a Rijke's tube results in a first-order neutral delay differential equation (NDDE). In this work, the NDDE governing the TAI is converted to a partial differential equation (PDE) and then into a system of ordinary differential equations (ODEs) using Galerkin approximations. A new pseudo inverse method, is proposed to handle the boundary conditions in the Galerkin method. The stability results obtained using our method are validated using the data from the literature.

Peer-review under responsibility of organizing committee of the IUTAM Symposium on Nonlinear and Delayed Dynamics of Mechatronic Systems

Keywords: Thermo-acoustic instability; Neutral delay differential equations; Rijke tube; Pseudo-inverse method, Galerkin approximations

1. Introduction

In closed cylindrical combustion chambers, flame dynamics and acoustics interact in a complex manner, and for certain parameter ranges, this interaction leads to TAI. According to Rayleigh, TAI develops in a combustion chamber due to the interaction between the acoustic waves generated from the unsteady heat release and the heat source [1]. When TAI occurs, the flame inside the combustion chamber oscillates violently and generates a loud noise; this leads to a sub-optimal performance of the combustion chamber. Also, the resulting high-frequency acoustic waves can cause fatigue damage to the combustion chamber, leading to its mechanical failure. Therefore, it is very important to design the combustion chamber in such a way that it will never encounter TAI during its operation. Many times, the existence of TAI in the combustion chambers is found at the final stages of its development, and therefore leaves a small room for any design modifications [2]. Therefore it is important to develop a mathematical model of the combustion chamber for predicting the TAI. This mathematical model can then be used to design the combustion chambers efficiently. Due to the multiphysics nature of the problem, developing a mathematical model for TAI is challenging. Over the years, many researchers have developed and studied simple thermo-acoustic devices like Rijke tube to understand TAI [3,4,5,6]. Dowling and Morgans [3] presented an exhaustive literature of the TAI and studied the problem from a

* Corresponding author. Tel.: +91-40-2301-7070.
E-mail address: vcprakash@iith.ac.in

Peer-review under responsibility of organizing committee of the IUTAM Symposium on Nonlinear and Delayed Dynamics of Mechatronic Systems
doi:10.1016/j.piutam.2017.08.023

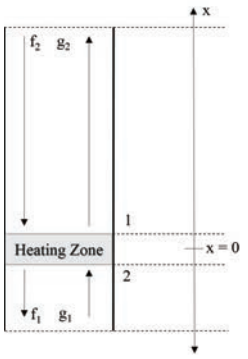

Fig. 1. Schematic representation of the combustion chamber

feedback control perspective. Dowling and Morgans[3,7] and Evesque[8] developed an analytical model for predicting TAI. They represented the dynamics of TAI using a delay differential equation (DDE) with rationally independent delays. It was found that the complex dynamics of the flame and its shape will also play a role in the TAI[4,9]. It should be noted that TAI can also occur in combustion chambers with electrical resistance as the heat source[5,10,11].

Subramanian et al.[12,13] developed a nonlinear DDE model for predicting the TAI in a Rijke tube. Different bifurcation diagrams were generated for understanding the behavior of the system. Olgac et al.[14,15] used the linearised model established by Dowling and Morgans[3] and developed a simple 1-D mathematical model of the TAI and is a neutral DDE (NDDE). In NDDEs, the delays exist even in the highest order derivative of the differential equation[16]. The delays in the mathematical models[3,14,15] appear due to finite propagation times of pressure waves in the upstream and downstream side of the combustion chamber. Olgac et al.[14,15,17] used a novel tool called "cluster treatment of characteristic roots" (CTCR) for determining the stability of these NDDEs. In this work the same mathematical model developed by Dowling and Morgans[3] and Olgac et al.[14,15] is used. The key scientific contribution of this work is towards constructing the stability analysis of the TAI in a Rijke's tube in the presence of multiple delays. Stability charts are constructed for the resultant DDEs using the pseudo-inverse method combined with Galerkin approximations. In this work, the NDDE is converted into a PDE along with a linear boundary condition. By using Galerkin approximation[18], the PDE is converted into a system of ODEs. A new pseudo-inverse method is then developed to handle the boundary condition of the PDE while developing ODE approximations for the NDDE. Once the NDDE is converted into system of ODEs the stability of the system can be easily studied.

2. Mathematical modelling

For completeness, we re-derive the TAI model developed by Dowling and Morgans[3,7] and Olgac et al.[14,15]. The schematic representation of the combustion chamber is shown in Fig. 1. The derivation of the model is divided into three sub-models, thermo-fluidic structure, acoustic behavior, and thermo-acoustic interface, and later all these sub-models are unified. The assumptions considered from the previous works[3,8] are the air flow is induced by natural buoyancy and is considered to be laminar along the tube. The ideal gas equations govern air in the tube and heat release zone is assumed to be infinitesimally thin and small compared to the acoustic wavelength.

2.1. Thermo-fluidic interface

With the above-mentioned assumptions, the fundamental equations for continuity, conservation of momentum, and conservation of energy for a thermo-fluidic segment can be written as:

$$\rho_1 u_1 = \rho_2 u_2, \quad p_2 + \rho_2 u_2^2 = p_1 + \rho_1 u_1^2, \quad \text{and} \quad \left(c_p T_2 + \frac{1}{2}u_2^2\right)\rho_2 u_2 A = \left(c_p T_1 + \frac{1}{2}u_1^2\right)\rho_1 u_1 A + Q. \tag{1}$$

Here ρ_1 and ρ_2 are the specific masses at the two cross-sections (see Fig. 1), u_1 and u_2 are the air speeds, c_p is the isobaric specific heat capacity, p_1 and p_2 are the pressures, T_1 and T_2 are the absolute temperatures, A is the cross-sectional area of the heating zone and Q is the heat release within the control volume (volume enclosed between the heat release zone). As stated above, the ideal gas relations that govern the dynamics of air are:

$$p = \rho R_s T, \qquad \frac{c_p}{c_v} = \gamma, \qquad c_p - c_v = R_s, \qquad c_p = \frac{\gamma}{\gamma - 1} R_s. \tag{2}$$

Where R_s is the specific gas constant, c_v is the constant volume specific heat and γ is the heat capacity ratio. Considering the assumptions stated earlier, important parameters that can be linearized in the current study are p, ρ and u, given by

$$p_i = \bar{p}_i + \tilde{p}_i, \qquad u_i = \bar{u}_i + \tilde{u}_i, \qquad \rho_i = \bar{\rho}_i + \tilde{\rho}_i, \qquad i = 1, 2, \tag{3}$$

where "–" is the average value and "∼" is the variational quantities. Substituting equation (3) in equation (1) and then linearising the resulting equations, we obtain

$$(\bar{\rho}_1 \bar{u}_2 - 2\bar{\rho}_1 \bar{u}_1)\tilde{u}_1 + (\bar{\rho}_1 \bar{u}_1)\tilde{u}_2 + (\bar{u}_1 \bar{u}_2 - \bar{u}_1^2)\tilde{\rho}_2 + \tilde{p}_2 - \tilde{p}_1 = 0, \tag{4a}$$

$$\frac{\gamma}{\gamma - 1}\bar{u}_2 \tilde{p}_2 - \frac{\gamma}{\gamma - 1}\bar{u}_1 \tilde{p}_1 + \frac{\gamma}{\gamma - 1}\bar{p}_2 + \bar{\rho}_1 \bar{u}_1 \bar{u}_2 - \left(\frac{\gamma}{\gamma - 1}\bar{p}_1 + \frac{3}{2}\bar{\rho}_1 \bar{u}_1^2 - \frac{1}{2}\bar{\rho}_1 \bar{u}_2^2\right)\tilde{u}_1 + \left(\frac{1}{2}\bar{u}_1 \bar{u}_2^2 - \frac{1}{2}\bar{u}_1^3\right)\tilde{\rho}_1 = \frac{\tilde{Q}}{A}. \tag{4b}$$

2.2. Acoustic behavior

It is known that the acoustic waves and heat release dynamics mutually interact with each other[1]. Hence, a disturbance in the heat release influences the acoustic waves that are generated in the tube, which means that a disturbance in Q influences u and p. From the assumptions stated in Olgac et al.[14], it can be deduced that the disturbance in Q results in local pressure and velocity perturbations. These pressure perturbations travel to both ends of the tube and reflect back to their starting point and influence the local velocities and pressures. This results in unsteady heat release. Here, the connection between the unsteady heat release dynamics and the acoustic waves is the pressure fluctuation. The evolution of sound pressure in the Rijke tube is governed by the following wave equation:

$$\frac{\partial^2 \tilde{p}}{\partial x^2} - \frac{1}{c^2}\frac{\partial^2 \tilde{p}}{\partial t^2} = 0, \tag{5}$$

where, c is the speed of sound, x is the position and t is the time. Using the d'Alembert's solution, the pressure fluctuations can be expressed as:

$$\tilde{p}_i(x,t) = f_j\left\{t - \frac{x}{c_j}\right\} + g_j\left\{t + \frac{x}{c_j}\right\}, \qquad i = u, d, \qquad j = 1, 2, \tag{6}$$

where f_j and g_j are any arbitrary functions that satisfy the initial and boundary conditions, u and d denote upstream ($-x_u < x < 0$) and downstream ($0 < x < x_d$) sides. Since it is assumed that the air flow in the tube is induced by the natural buoyancy ($\bar{c} >> \bar{u}$), the density and velocity variations can be written as:

$$\tilde{\rho}_i = \frac{1}{\bar{c}_j^2}\left[f_j(t - \frac{x}{\bar{c}_j}) - g_j(t + \frac{x}{\bar{c}_j})\right], \qquad \tilde{u}_i(t,x) = \frac{1}{\bar{\rho}_i \bar{c}_j}\left[f_j\left\{t - \frac{x}{c_j}\right\} - g_j\left\{t + \frac{x}{c_j}\right\}\right], \qquad i = u, d, \qquad j = 1, 2, \tag{7}$$

where, $\bar{c}_u$ and $\bar{c}_d$ are the upstream ($-x_u < x < 0$) and downstream ($0 < x < x_d$) wave speeds respectively. Since, it is assumed that the fluctuations in absolute temperature are at least an order of magnitude smaller than pressure and velocity variations, $\bar{c}_u$ and $\bar{c}_d$ are taken to be constant throughout.

2.3. Thermoacoustic interface

In this segment, the models developed for the thermo-fluidic interface and the acoustic behavior are connected. Boundary conditions for an open-ended Rijke tube are given by:

$$f_1(t) = -R_u g_1(t - \frac{2x_u}{\bar{c}_1}) \qquad g_2(t) = -R_d f_1(t - \frac{2x_d}{\bar{c}_2}) \qquad R_u, R_d < 1. \tag{8}$$

Where R_u, R_d are the acoustic pressure reflection coefficients at the upstream and downstream ends respectively. The variational form of expressions of p_i, u_i and ρ_i $(i = u, d)$ are now combined with equations (1)-(3). Then, the boundary conditions are substituted and the thermo-acoustic coupling is represented in the Laplace domain as follows:

$$(\mathbf{X} + \mathbf{YR})\begin{bmatrix} G \\ H \end{bmatrix} = \frac{\tilde{Q}(s)}{A\bar{c}_1}\begin{bmatrix} 0 \\ 1 \end{bmatrix} \tag{9}$$

where $G(s) = \mathscr{L}[g_1(t)]$, $H(s) = \mathscr{L}[f_2(t)]$, $\tilde{Q}(s) = \mathscr{L}[Q(t) - \bar{Q}]$, here, $\mathscr{L}$ is the Laplace transform, $\tau_u = 2x_u/c_1$, $\tau_d = 2x_d/c_2$ are the round-trip travel times of acoustic waves, $\mathbf{R} = \text{diag.}(R_u e^{-\tau_u s}, R_d e^{-\tau_d s})$ and $\mathbf{X}$, $\mathbf{Y}$ are given as:

$$\mathbf{X} = \begin{bmatrix} -1 + \bar{M}_1(2 - \frac{\bar{u}_2}{\bar{u}_1}) - \bar{M}_1^2(1 - \frac{\bar{u}_2}{\bar{u}_1}) & 1 + \bar{M}_1\frac{\bar{\rho}_1\bar{c}_1}{\bar{\rho}_2\bar{c}_2} \\ \bar{M}_1^2 - \frac{\bar{M}_1^2(1-\bar{M}_1)\left(\frac{\bar{u}_2^2}{\bar{u}_1^2}-1\right)}{2} + \frac{1-\gamma\bar{M}_1}{\gamma-1} & \bar{M}_1\bar{M}_2\frac{\bar{\rho}_1}{\bar{\rho}_2} + \frac{\bar{c}_2}{c_1}\frac{1+\gamma\bar{M}_2}{\gamma-1} \end{bmatrix} \quad \mathbf{Y} = \begin{bmatrix} 1 + \bar{M}_1(2 - \frac{\bar{u}_2}{\bar{u}_1}) + \bar{M}_1^2(1 - \frac{\bar{u}_2}{\bar{u}_1}) & -1 + \bar{M}_1\frac{\bar{\rho}_1\bar{c}_1}{\bar{\rho}_2\bar{c}_2} \\ \bar{M}_1^2 - \frac{\bar{M}_1^2(1+\bar{M}_1)\left(\frac{\bar{u}_2^2}{\bar{u}_1^2}-1\right)}{2} + \frac{1+\gamma\bar{M}_1}{\gamma-1} & \bar{M}_1\bar{M}_2\frac{\bar{\rho}_1}{\bar{\rho}_2} + \frac{\bar{c}_2}{c_1}\frac{1-\gamma\bar{M}_2}{\gamma-1} \end{bmatrix} \tag{10}$$

The causal relationship between the thermal input $\tilde{Q}$ and the acoustic outputs G and H can be clearly observed in equation (9).

2.4. Complete TAI model

A definite analytical relation that defines the causal nature between the heat release fluctuation $\tilde{Q}$ and the velocity fluctuations $\tilde{u}$ does not exist[11,19]. Therefore, the causal nature can be empirically represented by a transfer function $\phi(s)$, given as, $\phi(s) = \tilde{Q}(s)/\tilde{U}_1(s) = a/(bs + 1)$, where, $\tilde{U}_1(s) = \mathscr{L}[u_1(t)]$ is the Laplace transform, a and b are considered to be the DC gain and the time constant respectively that depend on the physical parameters of the geometry of the flame, mean heat release $(\bar{Q})$ and mean flow rate $(\bar{u})$[11,14]. The complete TAI dynamics obtained after substituting for $\phi(s)$ in equation (9) can be written as follows:

$$\begin{bmatrix} X_{11} + Y_{11}R_u e^{-\tau_u s} & X_{12} + Y_{12}R_d e^{-\tau_d s} \\ X_{21} + Y_{21}R_u e^{-\tau_u s} + \phi(s)\frac{R_u e^{-\tau_u s}+1}{A\bar{\rho}_1\bar{c}_1^2} & X_{22} + Y_{22}R_d e^{-\tau_d s} \end{bmatrix}\begin{bmatrix} G \\ H \end{bmatrix} = \mathbf{M}(s)\begin{bmatrix} G \\ H \end{bmatrix} = 0. \tag{11}$$

Equation (11) clearly indicates that the TAI model in a Rijke tube is a coupled DDE with independent time delays. The stability of equation (11) can be determined by the roots of the characteristic equation:

$$\det(\mathbf{M}) = \left((X_{11} + Y_{11}R_u e^{-\tau_u s})(X_{22} + Y_{22}R_d e^{-\tau_d s})\right) - \left((X_{21} + Y_{21}R_u e^{-\tau_u s} + \phi(s)\frac{R_u e^{-\tau_u s} + 1}{A\bar{\rho}_1\bar{c}_1^2})(X_{12} + Y_{12}R_d e^{-\tau_d s})\right) = 0. \tag{12}$$

Equation (12) represents the characteristic equation of the following DDE:

$$a_1\dot{x}(t) + a_2\dot{x}(t - \tau_u) + a_3\dot{x}(t - \tau_d) + a_4\dot{x}(t - \tau_{ud}) = b_1x(t) + b_2x(t - \tau_u) + b_3x(t - \tau_d) + b_4x(t - \tau_{ud}), \tag{13}$$

where $\tau_{ud} = \tau_u + \tau_d$, $a_1 = A\bar{\rho}_1\bar{c}_1^2b(X_{11}X_{22} - X_{12}X_{21})$, $a_2 = A\bar{\rho}_1\bar{c}_1^2b(X_{22}Y_{11} - X_{12}Y_{21})R_u$, $a_3 = A\bar{\rho}_1\bar{c}_1^2b(X_{11}Y_{22} - X_{21}Y_{12})R_d$, $a_4 = A\bar{\rho}_1\bar{c}_1^2b(Y_{11}Y_{22} - Y_{12}Y_{21})R_uR_d$, $b_1 = (X_{11}X_{22}A\bar{\rho}_1\bar{c}_1^2 - X_{12}X_{21}A\bar{\rho}_1\bar{c}_1^2 - X_{12}a)$, $b_2 = (X_{22}Y_{11}A\bar{\rho}_1\bar{c}_1^2 - X_{12}Y_{21}A\bar{\rho}_1\bar{c}_1^2 - X_{12}a)R_u$, $b_3 = (X_{11}Y_{22}A\bar{\rho}_1\bar{c}_1^2 - X_{21}Y_{12}A\bar{\rho}_1\bar{c}_1^2 - Y_{12}a)R_d$, and $b_4 = (Y_{11}Y_{22}A\bar{\rho}_1\bar{c}_1^2 - Y_{12}Y_{21}A\bar{\rho}_1\bar{c}_1^2 - Y_{12}a)R_uR_d$. It is easy to see that equation (13) is an NDDE. In this work, to determine the stability of such a class of equations, a novel pseudo-inverse method is proposed. Without actually constructing the physical model of the combustion chamber, the influence of geometrical parameters and delays on TAI can be studies using the proposed technique.

3. Characteristic roots using Galerkin approximations

For the ease of understanding and clarity, the current formulation is developed for a first-order NDDE. The proposed methodology can be easily extended to the higher-order NDDEs. As described in section 2, the dynamics of TAI in a Rijke tube is governed by equation (13). Substituting $x(t) = e^{\lambda t}$ in equation (13), results in the following transcendental equation

$$C(\lambda) = (a_1 + a_2e^{-\lambda\tau_u} + a_3e^{-\lambda\tau_d} + a_4e^{-\lambda\tau_{ud}})\lambda - b_1 - b_2e^{-\lambda\tau_u} - b_3e^{-\lambda\tau_d} - b_4e^{-\lambda\tau_{ud}} = 0. \tag{14}$$

Equation (14) is a quasi-polynomial and is exactly same as equation (12) and admits infinitely many roots. The system is stable if all the roots of the characteristic equation lie in the left half of the complex plane. But to verify the location of all the roots of equation (14) is a tedious task. To overcome this computationally intensive task, the stability of an approximation of the DDE (13) is considered. First, we introduce the transformation, $y(s,t) = x(t+s)$, where y is a function of s and t, $s \in [-\tau, 0]$ and $\tau = \max[\tau_u, \tau_d]$. Differentiating $y(s,t) = x(t+s)$ partially with respect to s and t gives:

$$\frac{\partial y(s,t)}{\partial s} = \frac{\partial y(s,t)}{\partial t}, \tag{15}$$

Boundary relations are obtained by substituting $s = 0$ and $s = -\tau$ in the transformation $y(s,t) = x(t+s)$, which are $y(0,t) = x(t)$ and $y(-\tau,t) = x(t-\tau)$. Substituting these boundary relations in equation (13), we get:

$$a_1\frac{\partial y(0,t)}{\partial t} + a_2\frac{\partial y(-\tau_u,t)}{\partial t} + a_3\frac{\partial y(-\tau_d,t)}{\partial t} + a_2\frac{\partial y(-\tau_{ud},t)}{\partial t} = b_1 y(0,t) + b_2 y(-\tau_u,t) + b_3 y(-\tau_d,t) + b_4 y(-\tau_{ud},t). \tag{16}$$

Equation (15) is a PDE and we approximate its solution $y(s,t)$ as:

$$y(s,t) = \sum_{i=1}^{N} \phi_i(s)\eta_i(t) = \boldsymbol{\phi}^T(s)\boldsymbol{\eta}(t), \tag{17}$$

where $\boldsymbol{\phi}(s) = [\phi_1(s), \phi_2(s), ..., \phi_N(s)]^T$ are the basis functions and $\boldsymbol{\eta}(t) = [\eta_1(t), \eta_2(t), ..., \eta_N(t)]$ are independent co-ordinates. We can represent the approximate solution using any complete set of basis functions (e.g., Chebyshev, Lagrange, and Hermite polynomials). Due to better convergence properties, in this study we used shifted Legendre polynomial as the basis functions[20], which is given as:

$$\phi_1(s) = 1, \qquad \phi_2(s) = 1 + \frac{2s}{\tau}, \qquad \phi_k(s) = \frac{(2k-3)\phi_2(s)\phi_{k-1}(s) - (k-2)\phi_{k-2}(s)}{k-1}, \quad k = 3, 4, ..., N. \tag{18}$$

Substituting equation (17) into equation (15), we obtain:

$$\boldsymbol{\phi}^T(s)\dot{\boldsymbol{\eta}}(t) = \boldsymbol{\phi}^T(s)'\boldsymbol{\eta}(t), \tag{19}$$

where $\boldsymbol{\phi}^T(s)' = \partial\boldsymbol{\phi}^T(s)/\partial s$. Pre-multiplying equation (19) by $\boldsymbol{\phi}(s)$ and integrating over $s \in [-\tau, 0]$, we arrive at the following set of ODEs:

$$\mathbf{C}\dot{\boldsymbol{\eta}}(t) = \mathbf{D}\boldsymbol{\eta}(t), \qquad \mathbf{C} = \int_{-\tau}^{0} \boldsymbol{\phi}(s)\boldsymbol{\phi}(s)^T ds, \qquad \mathbf{D} = \int_{-\tau}^{0} \boldsymbol{\phi}(s)\boldsymbol{\phi}'(s)^T ds. \tag{20}$$

The use of shifted Legendre polynomials as global shape functions allows us to express the entries of $\mathbf{C}$ and $\mathbf{D}$ in closed form as follows:

$$\mathbf{C}_{ii} = \frac{\tau}{2i-1}, \quad \mathbf{D}_{ij} = \begin{cases} 2, & \text{if} \quad i \le j \quad \text{and} \quad i+j \quad \text{is odd} \\ 0, & \text{otherwise} \end{cases} \qquad i, j = 1, 2, ..., N; \quad \tau = \max[\tau_1, \tau_1, ..., \tau_q]. \tag{21}$$

We now use the pseudo-inverse method to incorporate the boundary conditions. Pseudo-inverse method differs from that of the spectral-tau and spectral least-squares in the way the boundary conditions are incorporated into the formulation. Boundary conditions are obtained by substituting equation (17) in equation (16). The corresponding boundary conditions are:

$$c\dot{\boldsymbol{\eta}} = d\boldsymbol{\eta}, \tag{22}$$

where $c = a_1\boldsymbol{\phi}^T(0) + a_2\boldsymbol{\phi}^T(-\tau_u) + a_3\boldsymbol{\phi}^T(-\tau_d) + a_4\boldsymbol{\phi}^T(-\tau_{ud})$ and $d = b_1\boldsymbol{\phi}^T(0) + b_2\boldsymbol{\phi}^T(-\tau_u) + b_3\boldsymbol{\phi}^T(-\tau_d) + b_4\boldsymbol{\phi}^T(-\tau_{ud})$. Combining equation (20) and equation (22), we get,

$$\mathbf{M}\dot{\boldsymbol{\eta}}(t) = \mathbf{K}\boldsymbol{\eta}(t). \tag{23}$$

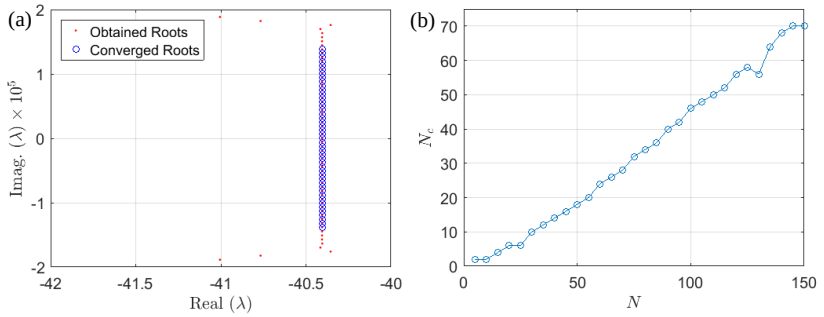

Fig. 2. For parameters $a = 133.25$ and $b = 0.0003$, (a) Characteristic roots for $N = 100$, (b) No. of converged roots with increasing N.

where $\mathbf{M} = [\mathbf{C}\ \ \bar{\mathbf{c}}]^T$ and $\mathbf{K} = [\mathbf{D}\ \ \bar{\mathbf{d}}]^T$. Equation (23) is an over-deterministic system of $N+1$ equations in N unknowns in $\dot{\boldsymbol{\eta}}(t)$, the least square solution for $\dot{\boldsymbol{\eta}}(t)$ is given by:

$$\dot{\boldsymbol{\eta}}(t) = \mathbf{A}\boldsymbol{\eta}(t), \tag{24}$$

where $\mathbf{A} = \mathbf{M}^{+}\mathbf{K}$ and $\mathbf{M}^{+}$ is the Moore-Penrose inverse of $\mathbf{M}$. Equation (24) represents a finite dimensional ODE approximation for the DDE (equation (13)). The stability of equation (13) can now be studied by using equation (24). In fact the eigenvalues of $\mathbf{A}$ approximate the characteristic roots of equation (14) and as we increase the number (N) of approximating ODEs in equation (24), more and more eigenvalues of $\mathbf{A}$ converge to the characteristic roots of equation (14).

4. Results and Discussions

For the first test case, seven different combinations of a and b are considered and are same as those reported by Olgac et al.[14,15]. The numerical values of other parameters are $R_u = 0.98$, $R_d = 0.98$, $\gamma = 1.4$, $A = 0.0028\ m^2$, $\bar{\rho}_i = 1.2\ kg/m^3$ and $c_i = 358\ m/s$. For the second test case, we select $a = 200$, $b = 0.002$, $R_u = 0.93$, $R_d = 0.93$, $\gamma = 1.4$, $A = 0.00075\ m^2$, $\bar{\rho}_i = 1.2\ kg/m^3$ and $c_i = 340\ m/s$. Figure 2a shows the characteristic roots of the NDDE given by equation (14) for $a = 133.25$, $b = 0.0003$, $N = 100$, $\tau_u = 0.0005$ and $\tau_d = 0.0005$, for which the system is stable. For $N = 100$, the size of $\mathbf{A}$ is 100×100. The eigenvalues $\hat{\lambda}_k$, $k = 1, 2, 3, ..., N$ of $\mathbf{A}$ approximate the characteristic roots of equation (14). Red dots in Fig. 2a represent the eigenvalues of $\mathbf{A}$, blue circles represent those eigenvalues of $\mathbf{A}$ that converged to the characteristic roots of equation (14). To understand how the eigenvalues of $\mathbf{A}$ converge to the characteristic roots of equation (14), we define the absolute error, ϵ_k, as $\epsilon_k = \left|C(\hat{\lambda}_k)\right|, k = 1, 2, ..., N$. A particular eigenvalue of $\mathbf{A}$ is considered to be converged to the characteristic root of equation (14) if $\epsilon_k < 10^{-4}$. It is clear from Fig. 2a, that the rightmost roots are the first to converge and this is due to the spectral nature of discretization used for converting the DDE into a system of ODEs. Fig. 2b shows the number of converged eigenvalues (N_c) of $\mathbf{A}$ as a function of N and we observe that $N_c \approx N/2$.

In Figs. [3-5], red color represents the stability region obtained by using the pseudo-inverse method and the blue borders represent the stability boundaries obtained from the works of Olgac et al.[14,15]. Figure 3a shows the stability diagram in the $[\tau_u, \tau_d]$ space for the first test case with $a = 133.25$ and $b = 0.0003$. Figure 3b shows the stability diagram in the $[x_u, x_d]$ space for the parameters of second test case with $a = 200$ and $b = 0.02$. From Fig. 3 it is clear that our results are in close agreement to those obtained by Olgac et al.[14,15].

Next, the influence of transfer function parameters, a and b, on the TAI in a Rijke tube is studied. The first study was to vary a with $b = 0.0004$. The second study was to vary b with $a = 135$. Figure 4 shows the influence of increasing a on the stability of TAI. Figure 5 shows the influence of increasing b on the stability of TAI. All the stability charts obtained by using the pseudo-inverse method are in very close agreement with those obtained by Olgac et al.[14]. One important observation that can be made from Figs. [4-5] is that the area of stability region of TAI is inversely proportional to a and directly proportional to b, for a given set of parameters of the Rijke tube.

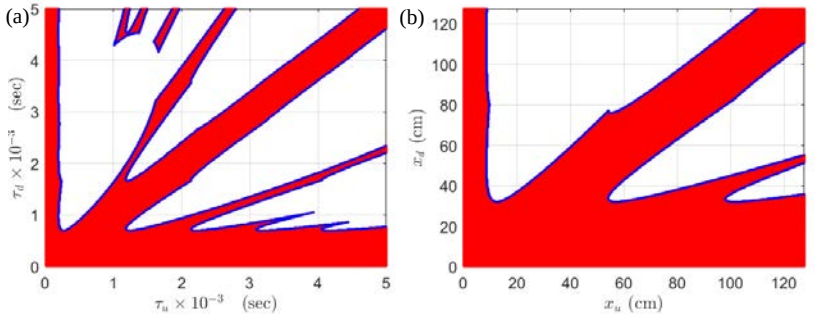

Fig. 3. Stability diagrams for (a) $a = 133.25$ and $b = 0.0003$, (b) $a = 200$, $b = 0.002$.

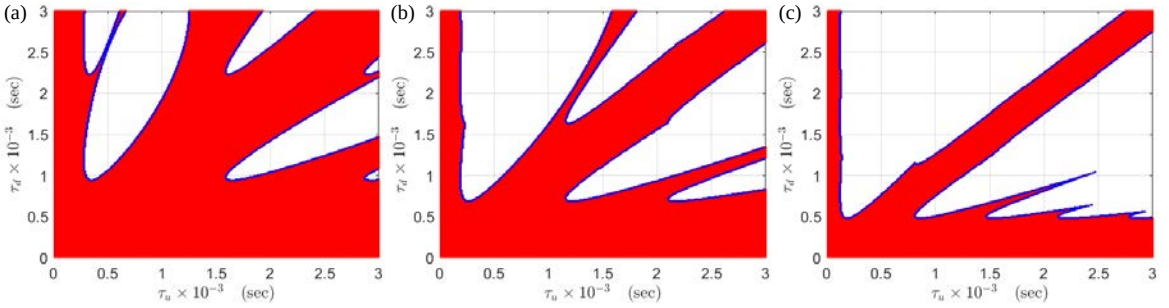

Fig. 4. Influence of the transfer function parameter a with $b = 0.0004$ on the stability of TAI. (a) $a = 110$, (b) $a = 135$, (c) $a = 180$.

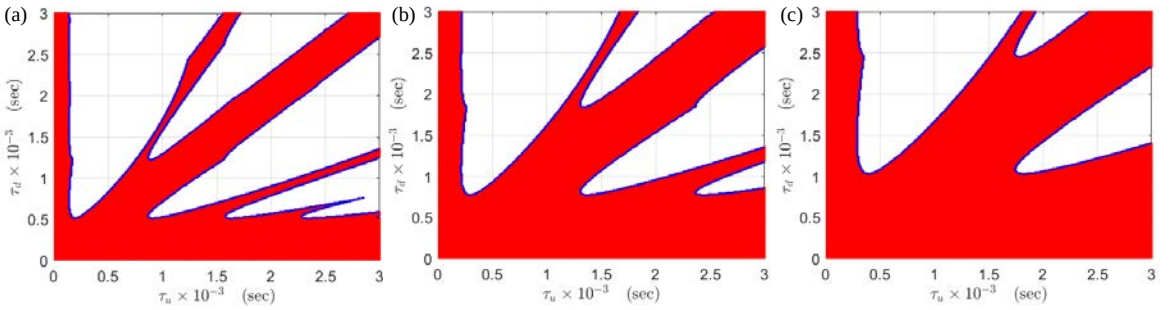

Fig. 5. Influence of the transfer function parameter b with $a = 135$ on the stability of TAI. (a) $b = 0.0003$, (b) $b = 0.00045$, (c) $b = 0.0006$.

5. Conclusions and Future work

In this paper, a simple Rijke tube model is used to study the complex dynamics of TAI. From the existing literature, a linearized NDDE model of TAI is revisited. We converted the NDDE model into a system of ODEs using Galerkin approximations. A new pseudo-inverse technique for handling the boundary conditions in Galerkin approximations is proposed. The developed theory is applied to obtain the stability regions for the TAI and are found to be in good agreement. The stability charts can be used to avoid TAI while designing the combustion chamber. The main advantage of the proposed method is that the stability theory of ODEs can be directly applied to study the stability of NDDEs. It was found that approximately $N/2$ number of rightmost eigenvalues of approximating ODEs (of dimension N) converged to the characteristic roots of NDDE. Our pseudo-inverse method is easier in formulation compared to the Lagrange multiplier and spectral-tau methods. The proposed methodology can be easily extended to higher-order NDDEs.

Acknowledgements

CPV gratefully acknowledges the Department of Science and Technology for funding this research through Inspire fellowship (DST/INSPIRE/04/2014/000972).

References

1. Rayleigh, L. The explanation of certain acoustic phenomena. *Nature* 1878;**18**.
2. Cazalens, Michel; Roux, Sébastien; Sensiau, Claude and Poinsot, Thierry. Combustion instability problems analysis for high-pressure jet engine cores. *Journal of Propulsion and Power* 2008;**24**:770–778.
3. Dowling, Ann P and Morgans, Aimee S. Feedback control of combustion oscillations. *Annual Reviews in Fluid Mechanics* 2005;**37**:151–182.
4. Selimefendigil, F; Sujith, RI and Polifke, Wolfgang. Identification of heat transfer dynamics for non-modal analysis of thermoacoustic stability. *Applied Mathematics and Computation* 2011;**217**:5134–5150.
5. Bittanti, Sergio; De Marco, Antonio; Poncia, Guido and Prandoni, Walter. Identification of a model for thermoacoustic instabilities in a Rijke tube. *IEEE Transactions on control systems technology* 2002;**10**:490–502.
6. Kopitz, Jan and Polifke, Wolfgang. CFD-based application of the Nyquist criterion to thermo-acoustic instabilities. *Journal of Computational Physics* 2008,**227**:6754–6778.
7. Dowling, Ann P. Nonlinear self-excited oscillations of a ducted flame. *Journal of fluid mechanics* 1997;**346**:271–290.
8. Evesque, Stéphanie Marie-Noelle. Adaptive control of combustion oscillations. *PhD thesis, University of Cambridge* 2001.
9. Culick, FE and Kuentzmann, Paul. Unsteady motions in combustion chambers for propulsion systems. *DTIC Document* 2006.
10. Matveev, Konstantin. Thermoacoustic instabilities in the Rijke tube: experiments and modeling. *PhD thesis, California Institute of Technology* 2003.
11. Gelbert, Gregor; Moeck, Jonas P; Paschereit, Christian O and King, Rudibert. Feedback control of unstable thermoacoustic modes in an annular Rijke tube. *Control Engineering Practice* 2012;**20**:770–782.
12. Subramanian, Priya; Mariappan, Sathesh; Sujith, RI and Wahi, Pankaj. Bifurcation analysis of thermoacoustic instability in a horizontal Rijke tube. *International journal of spray and combustion dynamics* 2010;**2**:325–355.
13. Subramanian, Priya; Sujith, RI and Wahi, P. Subcritical bifurcation and bistability in thermoacoustic systems. *Journal of Fluid Mechanics* 2013;**715**: 210–238.
14. Olgac, Nejat; Cepeda-Gomez, Rudy; Zalluhoglu, Umut and Kammer, Ayhan S. Parametric investigation of thermoacoustic instability (TAI) in a rijke tube: a time-delay perspective. *International Journal of Spray and Combustion Dynamics* 2015;**7**:39–68.
15. Olgac, Nejat; Zalluhoglu, Umut and Kammer, Ayhan S. Predicting Thermoacoustic Instability: A Novel Analytical Approach and Its Experimental Validation. *Journal of Propulsion and Power* 2014;**30**:1005–1015.
16. Vyasarayani, C P. Galerkin Approximations for Neutral Delay Differential Equations. *Journal of Computational and Nonlinear Dynamics* 2013;**8**:021014.
17. Olgac, Nejat; Zalluhoglu, Umut and Kammer, Ayhan Sebastian. A new perspective in designing delayed feedback control for thermo-acoustic instabilities (TAI). *Combustion Science and Technology* 2015;**187**:697–720.
18. Vyasarayani, C P. Galerkin approximations for higher order delay differential equations. *Journal of Computational and Nonlinear Dynamics* 2012;**7**:031004.
19. Wu, Xuesong; Wang, Meng; Moin, Parviz and Peters, Norbert. Combustion instability due to the nonlinear interaction between sound and flame. *Journal of fluid mechanics* 2003;**497**:23–53.
20. Vyasarayani, C P; Subhash, S and Kalmár-Nagy, T. Spectral approximations for characteristic roots of delay differential equations. *International Journal of Dynamics and Control* 2014;**2**:126–132.